04,15

# Influence of uniaxial mechanical pressure on the characteristics of Lamb waves and SH waves in layered piezoelectric structures AI|AIN|diamond

© S.I. Burkov<sup>1</sup>, O.N. Pletnev<sup>1</sup>, P.P. Turchin<sup>1,2,¶</sup>, V.I. Turchin<sup>1</sup>

Krasnoyarsk, Russia

Received March 31, 2025 Revised May 16, 2025 Accepted May 19, 2025

The effect of uniaxial mechanical pressure on the dispersion characteristics of Lamb waves and SH-waves in multilayer piezoelectric structures is studied for different variants of uniaxial mechanical pressure application. The conditions of uniaxial mechanical pressure application are noted, under which changes in the phase velocities of Lamb waves and SH-waves are maximal or absent, which can be of great importance for the development of controlled acoustoelectronic devices.

Keywords: multilayer structures, aluminum nitride, hybridization, backward acoustic waves.

DOI: 10.61011/PSS.2025.06.61686.64-25

## 1. Introduction

Multilayer piezoelectric structures are currently used mainly for creating acoustoelectric devices [1] such as stripeline and matched filters [2] that are widely used in modern mobile communications systems; high temperature sensors, for example, langisite-crystal ones [3]; various types of pressure and humidity transducers [4,5], chemical substance concentration sensors [6,7], etc. Synthesis and investigation of new structures facilitate cost reduction and increase in the accuracy of such devices [8]. The interest in exploring the influence of uniaxial mechanical pressure is primarily driven by the fact that multilayer piezoelectric structures are synthesized under pressure to avoid fractures and damage, and this affects the elastic wave properties [9]. For example, in polyvinylidenfluoride (PVDF) structures with the  $0^{\circ}|\theta^{\circ}|0^{\circ}$  configuration, application of initial tension stress increases wave phase and group velocities, which induces displacement of the Lamb wave dispersion dependences [10]. Residual mechanical stress affects the electron and hole drift in piezoelectric semiconductors, and the magnitude of impact directly depends on the wave propagation direction [11]. In case of Love wave propagation in a viscoelastic medium, elastic wave attenuation without initial mechanical stress goes much faster than with initial mechanical stress [12]. When a uniaxial mechanical pressure of 100 MPa is applied to an aluminum plate and the wave propagates at 45° with respect to the applied pressure, interaction (hybridization) of the fundamental modes  $SH_0$  and  $S_0$  occurs [13].

Hybridization of two and more modes plays a critical role in elastic wave propagation leading to considerable modification of dispersion dependences of the most properties, in particular, the phase and group velocities [14]. However, few if any investigations have been conducted concerning the influence of mechanical pressure on a multilayer piezoelectric structure in the hybridization region.

Acoustic back waves characterized by opposite directions of phase velocity (PV) and acoustic wave energy flux, i.e. negative energy transfer group velocities, have recently drawn high interest of acoustoelectric device developers [15,16]. Existence of back waves was investigated theoretically and experimentally in isotropic plates [17], multilayer structures and phonon crystals [18,19]. PV dispersion dependence of the Lamb wave, part of which corresponds to the back wave, has a frequency band where the elastic Lamb wave has a zero group velocity (ZGV) [20,21]. Elastic wave modes with ZGV are special points on a dispersion curve where the group velocity vanishes, while PV is still finite, i.e. the wave vector of this mode is still finite [22]. Advantage of these acoustic wave modes in the ZGV point is in a combination of energy localization and high Q factor of the cavity. Many applications use these unique properties, in particular, a high-Q AlN membrane cavity at 2 GHz [23] in the ZGV region. Acoustic Lamb back wave excitation and recording procedure is addressed in [20,24], but the influence of external mechanical impacts on acoustic back waves was not investigated.

The paper studies the influence of uniaxial mechanical pressure on the properties of elastic

<sup>&</sup>lt;sup>1</sup> Siberian Federal University,

<sup>&</sup>lt;sup>2</sup> Kirensky Institute of Physics, Federal Research Center KSC SB, Russian Academy of Sciences, Krasnoyarsk, Russia

<sup>¶</sup> E-mail: pturchin@sfu-kras.ru

Lamb waves and SH-waves in multilayer piezoelectric Al|AlN|[110]diamond type structures.

# 2. Theory of elastic wave propagation in a piezoelectric-crystal plate exposed to external mechanical pressure

For small amplitude waves when the piezoelectric crystal is exposed to homogeneous mechanical pressure, equation of motion, equations of electrostatics and equations of state of the piezoelectric medium are written as [25]

$$\rho_{0}\ddot{\tilde{U}}_{A} = \tilde{\tau}_{AB,B} + \tilde{U}_{A,PQ}\overline{\tau}_{PQ};$$

$$\tilde{D}_{M,M} = 0;$$

$$\tilde{\tau}_{AB} = c_{ABCD}^{*}\tilde{\eta}_{CD} - e_{MAB}^{*}\tilde{E}_{M};$$

$$\tilde{D}_{M} = \varepsilon_{MN}^{*}\tilde{E}_{N} + e_{MAB}^{*}\tilde{\eta}_{AB},$$
(1)

where  $\rho_0$  is the density of crystal in the undeformed state,  $\tilde{\mathbf{U}}_A$  is the dynamic elastic displacement vector,  $\tau_{AB}$  is the thermodynamic stress tensor,  $\tilde{\mathbf{D}}_M$  electric flux density vector,  $\overline{\tau}_{PQ} = -\overline{\tau}\mathbf{P}_P\mathbf{P}_Q$  is the static uniaxial stress tensor,  $\mathbf{P}_Q$  and  $\mathbf{P}_P$  are pressure force unit vector components,  $\eta_{CD}$  is the strain tensor. Relation (1), as below, implies summation convention over reiterated coordinate indices.

Effective material tensors of moduli of elasticity, piezoelectric constants and permittivity in the approximation of linear dependence on static mechanical stress  $\overline{\tau}$  are written as [26]

$$C^*_{\text{ABKL}} = C^{\text{E}}_{\text{ABKL}} - C^{\text{E}}_{\text{ABKLQR}} S^{\text{E}}_{\text{QRMN}} P_{\text{M}} P_{\text{N}} \overline{\tau};$$

$$e^*_{\text{NAB}} = e_{\text{NAB}} - e_{\text{NABKL}} S^{\text{E}}_{\text{KLMN}} P_{\text{M}} P_{\text{N}} \overline{\tau};$$

$$\varepsilon^*_{\text{MN}} = \varepsilon^{\eta}_{\text{MN}} - H_{\text{NMAB}} S^{\text{E}}_{\text{ABKL}} P_{\text{K}} P_{\text{L}} \overline{\tau}.$$

$$(2)$$

Here,  $C_{\rm ABKL}^{\rm E}$ ,  $e_{\rm NAB}$ ,  $e_{\rm MN}^{\eta}$  are elastic piezoelectric and dielectric second-order constants;  $S_{\rm ABKL}^{\rm E}$  are elastic compliance constants;  $C_{\rm ABKLQR}^{\rm E}$ ,  $e_{\rm NABKL}$ ,  $H_{\rm NMAB}$  are nonlinear elastic piezoelectric and electrostriction material tensors, P are external mechanical pressure vector components.

Calculation was conducted in an arbitrary orthogonal coordinate system, the  $\mathbf{X}_3$  axis is oriented along the normal to the free layer surface, and the  $\mathbf{X}_1$  axis is oriented along the wave propagation direction. For normal components of the stress tensor of multilayer structures, equality to zero on the free layer surfaces is the boundary condition. Continuity of tangents to the interface surface of electric field strength vector components is provided by the electric potential continuity conditions at the layer—vacuum interface. In addition, normal stress tensor component equality condition and electric potential continuity at the layer interface shall be satisfied. For example, boundary conditions for a three-

layer structure will be written as [26]:

$$\tau_{3j}^{(1)} = 0|_{x_{3}=h_{3}}; D_{3}^{(1)} = D^{(\text{vac})}|_{x_{3}=h_{3}}; \varphi^{(1)} = \varphi^{(\text{vac})}|_{x_{3}=h_{3}};$$

$$\tau_{3j}^{(1)} = \tau_{3j}^{(2)}|_{x_{3}=h_{2}}; D_{3}^{(1)} = D_{3}^{(2)}|_{x_{3}=h_{2}}; \varphi^{(1)} = \varphi^{(2)}|_{x_{3}=h_{2}};$$

$$U_{A}^{(1)} = U_{A}^{(2)}|_{x_{3}=h_{2}};$$

$$\tau_{3j}^{(2)} = \tau_{3j}^{(3)}|_{x_{3}=h_{1}}; D_{3}^{(2)} = D_{3}^{(3)}|_{x_{3}=h_{1}}; \varphi^{(2)} = \varphi^{(3)}|_{x_{3}=h_{1}};$$

$$U_{A}^{(2)} = U_{A}^{(3)}|_{x_{3}=h_{1}};$$

$$\tau_{3j}^{(3)} = 0|_{x_{3}=0}; D_{3}^{(3)} = D^{(\text{vac})}|_{x_{3}=0}; \varphi^{(3)} = \varphi^{(\text{vac})}|_{x_{3}=0}.$$
(3)

When mechanical stresses are applied orthogonally to the  $(P \parallel X_3)$  free surface, elastic properties of the loading medium shall be taken into account. Assuming that the uniaxial stress takes place in such configuration without elastic contact with the free surface (for example, loading by gas medium), mechanical boundary conditions for this case may be written as

$$\tilde{\tau}_{3J} + \tilde{U}_{J,K} \tau_{3K} = 0(X3 = h3).$$
 (4)

The explicit form of boundary conditions (3) for a piezoelectric plate exposed to the uniaxial mechanical pressure is described in [27,28].

Elastic wave PV control coefficient  $\alpha_P$  with the applied uniaxial mechanical pressure is written as

$$\alpha_{\rm P} = \frac{1}{v_0} \left( \frac{\Delta v}{\Delta P} \right)_{\Lambda P \to 0} = \frac{1}{v_0} \left( \frac{v - v_0}{\Delta P} \right)_{\Lambda P \to 0}, \tag{5}$$

where  $v_0$  is the wave propagation velocity without interaction, v is the velocity at  $\Delta P$ .

# Lamb wave dispersion dependences for multilayer piezoelectric structures

The equations of motion were used to calculate the Lamb wave PV propagation in multilayer piezoelectric structures. In our case, the Al|AlN|[110]diamond structure was used as multilayer structures. Elastic waves in all cases propagated in the [100] orientation (along the  $\mathbf{X}_1$  axis of the arbitrary coordinate system) of the (001) plane for the piezoelectric crystal, but the diamond is oriented along the [110] direction of the (001) plane. Note that for the uniaxial mechanical pressure along the normal to the ( $\mathbf{P} \parallel \mathbf{X}_3$ ) free surface of the multilayer structure, the pressure was applied in such a way that the mechanical boundary conditions were not broken (4). All dispersion dependences are given depending on hf, where h is the piezoelectric layer thickness, and f is the wave propagation frequency.

Application of the external uniform mechanical pressure along the normal to the free surface, i.e.  $P \parallel X_3$ , to the Al|AlN|[110]diamond structure, according to the Curie principle, will change the initial symmetry of the diamond

crystal from cubic to tetragonal. Consequently, all existing material constants are modified:

$$C_{11}^{*} = C_{22}^{*} = C_{11}^{E} + [(C_{111} + C_{112})S_{12} + C_{112}S_{11}]\overline{\tau};$$

$$C_{12}^{*} = C_{12}^{E} + [C_{123}S_{11} + 2C_{112}S_{12}]\overline{\tau};$$

$$C_{13}^{*} = C_{23}^{E} = C_{12}^{E} + [C_{112}(S_{11} + S_{12}) + C_{123}S_{12}]\overline{\tau};$$

$$C_{33}^{*} = C_{11}^{E} + [C_{111}S_{11} + 2C_{112}S_{12}]\overline{\tau};$$

$$C_{44}^{*} = C_{55}^{*} = C_{44}^{E} + [C_{155}(S_{11} + S_{12}) + C_{144}S_{12}]\overline{\tau};$$

$$C_{66}^{*} = C_{44}^{E} + [C_{144}S_{11} + 2C_{155}S_{12}]\overline{\tau}.$$

However, third-order material constants are unknown for the AlN crystal, therefore the influence of the uniaxial mechanical pressure on the AlN crystal layer was considered only as geometrical nonlinearity, i.e. the static Green tensor

$$\overline{\eta}_{AB} = \delta_{AB} + 2S_{ABCD}\overline{\tau}_{CD};$$

$$\overline{\tau}_{CD} = -\overline{\tau}P_{C}P_{D} [25].$$

Thus, in this case the Green-Christoffel tensor, explicit form of which is given in [25], for the AlN layer in the elastic wave propagation direction  $\mathbf{X}_1$  considering the static Green tensor is written as:

$$\begin{split} &\Gamma_{11} = (C_{11}^{\rm E} + 2C_{11}^{\rm E}S_{13}\overline{\tau})k_1^2 + (C_{44}^{\rm E} + 2C_{44}^{\rm E}S_{13}\overline{\tau})k_3^2; \\ &\Gamma_{13} = \left(C_{13}^{\rm E} + C_{44}^{\rm E} + 2(C_{13}^{\rm E}S_{11} + C_{44}^{\rm E}S_{33})\overline{\tau}\right)k_1k_3; \\ &\Gamma_{22} = (C_{66}^{\rm E} + 2C_{66}^{\rm E}S_{13}\overline{\tau})k_1^2 + (C_{44}^{\rm E} + 2C_{44}^{\rm E}S_{13}\overline{\tau})k_3^2; \\ &\Gamma_{31} = \left(C_{44}^{\rm E} + \left(2(C_{44}^{\rm E}S_{33} + C_{13}^{\rm E}S_{13}) + 1\right)\overline{\tau}\right)k_1k_3; \\ &\Gamma_{33} = (C_{44}^{\rm E} + 2C_{44}^{\rm E}S_{33}\overline{\tau})k_1^2 + (C_{33}^{\rm E} + (2C_{33}^{\rm E}S_{33} + 1)\overline{\tau}\right)k_3^2; \\ &\Gamma_{41} = \left(e_{15} + e_{31} + 2(e_{15}S_{33} + e_{31}S_{13})\overline{\tau}\right)k_1k_3; \\ &\Gamma_{43} = \left(e_{15} - 2e_{15}S_{33}\overline{\tau}\right)k_1^2 + \left(e_{33} - 2e_{33}S_{33}\overline{\tau}\right)k_3^2; \\ &\Gamma_{14} = \left(e_{15} + e_{31}\right)k_1k_3; \\ &\Gamma_{14} = \left(e_{15} + e_{31}\right)k_1k_3; \\ &\Gamma_{34} = e_{15}k_1^2 + e_{33}k_3^2; \\ &\Gamma_{44} = \varepsilon_{11}k_1^2 + \varepsilon_{33}k_3^2; \\ &\Gamma_{12} = \Gamma_{21} = \Gamma_{23} = \Gamma_{32} = \Gamma_{42} = \Gamma_{24} = 0. \end{split}$$

Note that geometrical nonlinearity, i.e. geometrical layer distortion, is exhibited in this case, and of course the Green-Christoffel tensor (7) becomes nonsymmetric.

Figure 1 shows the dependences of Lamb waves and SH-waves, and of control coefficients (5) for the Al|AlN|[110]diamond structure for uniaxial mechanical pressure application cases along the wave propagation direction ( $\mathbf{P} \parallel \mathbf{X}_1$ ) orthogonally to the sagittal plane ( $\mathbf{P} \parallel \mathbf{X}_2$ ) and orthogonally to the free surface ( $\mathbf{P} \parallel \mathbf{X}_3$ ). The (001) plane of the piezoelectric AlN layer is isotropic with respect to elastic properties, therefore pure elastic wave modes propagate in this structure. The range of reviewed values depending on hf (h is the layer thickness, f is the wave frequency) is from 0 to 18 000 m/s (Figure 1). Relation

of the piezolayer thickness to the diamond thickness is 0.01, but the relation of the metal layer thickness to the piezoelectric thickness is 0.03. In particular, the Al|AlN|[110]diamond layer thicknesses, for example, may be equal to  $0.13|4.5|450\,\mu\text{m}$ . Only the Lamb waves have piezoelectric activity as shown in (7). Electromechanical coupling coefficients for the Al|AlN|[110]diamond multilayer structure are shown in [29].

Typical PV dispersion dependence for the antisymmetric (A) and symmetric (S) Lamb waves and SH-waves is shown in Figure 1, b. When external pressure is applied along the elastic wave propagation direction ( $\mathbf{P} \parallel \mathbf{X}_1$ ) for the fundamental Lamb wave, the maximum  $\alpha_p$  (5) of the symmetric mode S<sub>0</sub> is reached for thin crystal wafers, in particular, equal to  $4.2 \cdot 10^{-12} \,\mathrm{Pa}^{-1}$  at  $hf = 1850 \,\mathrm{m/s}$ . However, the maximum  $\alpha_p$  of the antisymmetric mode  $A_0$  is equal to  $\alpha_{\rm p}=1.9\cdot 10^{-12}\,{\rm Pa}^{-1}$  at  $hf=50\,{\rm m/s}$  (Figure 1, d). As hf increases, PV of the fundamental mode  $S_0$  of the Lamb wave tends to PV of 11141.9 m/s of the nondispersive surface Rayleigh acoustic wave (SAW), control coefficient of which is equal to  $\alpha_p = 1.95 \cdot 10^{-12} \, Pa^{-1}$  when the uniaxial mechanical pressure is applied along the  $X_1$  axis  $(P \parallel X_1)$ . Note that as hf increases, the fundamental mode  $A_0$  of the Lamb wave transforms into the Rayleigh mode R<sub>0</sub> that decays in the diamond crystal at hf > 3500 m/s, PV of which tends to the SAW velocity in the AlN crystal [30]. When the uniaxial mechanical pressure is applied orthogonally to the sagittal plane ( $\mathbf{P} \parallel \mathbf{X}_2$ ) for the fundamental modes  $S_0$  and  $A_0$ of the Lamb wave at hf > 3500 m/s, control coefficients  $\alpha_p$ are equal to  $1.08 \cdot 10^{-12}$  and  $1.1 \cdot 10^{-12} \, \text{Pa}^{-1}$ , respectively (Figure 1, e). However, when the uniaxial pressure is applied as  $P \parallel X_3$ , i.e. along the normal to the free surface, values of  $\alpha_p$  of the Lamb wave modes  $S_0$  and  $A_0$  differ more considerably (Figure 1, f). For example, at  $hf = 10\,000\,\text{m/s}$ they are  $9.6 \cdot 10^{-13}$  and  $1.3 \cdot 10^{-12} \, \text{Pa}^{-1}$ , respectively.

In the variation range from 11 590 m/s to 11 126 m/s, i.e. in the vicinity of the corresponding slow quasi-shear wave PV values, the PV dispersion dependence for SH<sub>0</sub> is weakly pronounced. Dispersion dependence of  $\alpha_p$  for SH<sub>0</sub> at  $\mathbf{P} \parallel \mathbf{X}_1$  is within the range from  $1 \cdot 10^{-12}$  to  $1.56 \cdot 10^{-12}$  Pa<sup>-1</sup> (Figure 1, d).

Dispersion dependence of  $\alpha_p$  for a higher-order Lamb wave, when the mechanical pressure  $\mathbf{P} \parallel \mathbf{X}_1$  or  $\mathbf{P} \parallel \mathbf{X}_2$  is applied for symmetric  $S_n$   $(n=1,2,\ldots)$  and antisymmetric An, is from  $3.3 \cdot 10^{-12}$  to  $1.56 \cdot 10^{-12} \, \mathrm{Pa}^{-1}$  of the fast quasi-shear wave (QFS) of the diamond at  $\mathbf{P} \parallel \mathbf{X}_1$ . For the elastic wave modes  $\mathrm{SH}_n$ , the  $\alpha_p$  variation range is from  $3.0 \cdot 10^{-12}$  to  $1.1 \cdot 10^{-12} \, \mathrm{Pa}^{-1}$  of the slow quasi-shear wave (QSS) of the diamond at  $\mathbf{P} \parallel \mathbf{X}_1$  (Figure 1, d). The same is also true when the mechanical pressure  $\mathbf{P} \parallel \mathbf{X}_2$  is applied, but the range of  $\alpha_p$  for the Lamb wave modes is from  $2.6 \cdot 10^{-12}$  to  $1.51 \cdot 10^{-12} \, \mathrm{Pa}^{-1}$  (Figure 1, e).

In the Al|AlN|[110]diamond multilayer structure, there is no hybridization effect in the elastic wave mode PV range below the longitudinal bulk acoustic wave (BAW) values (Figure 1, b). However, in the standing wave region,

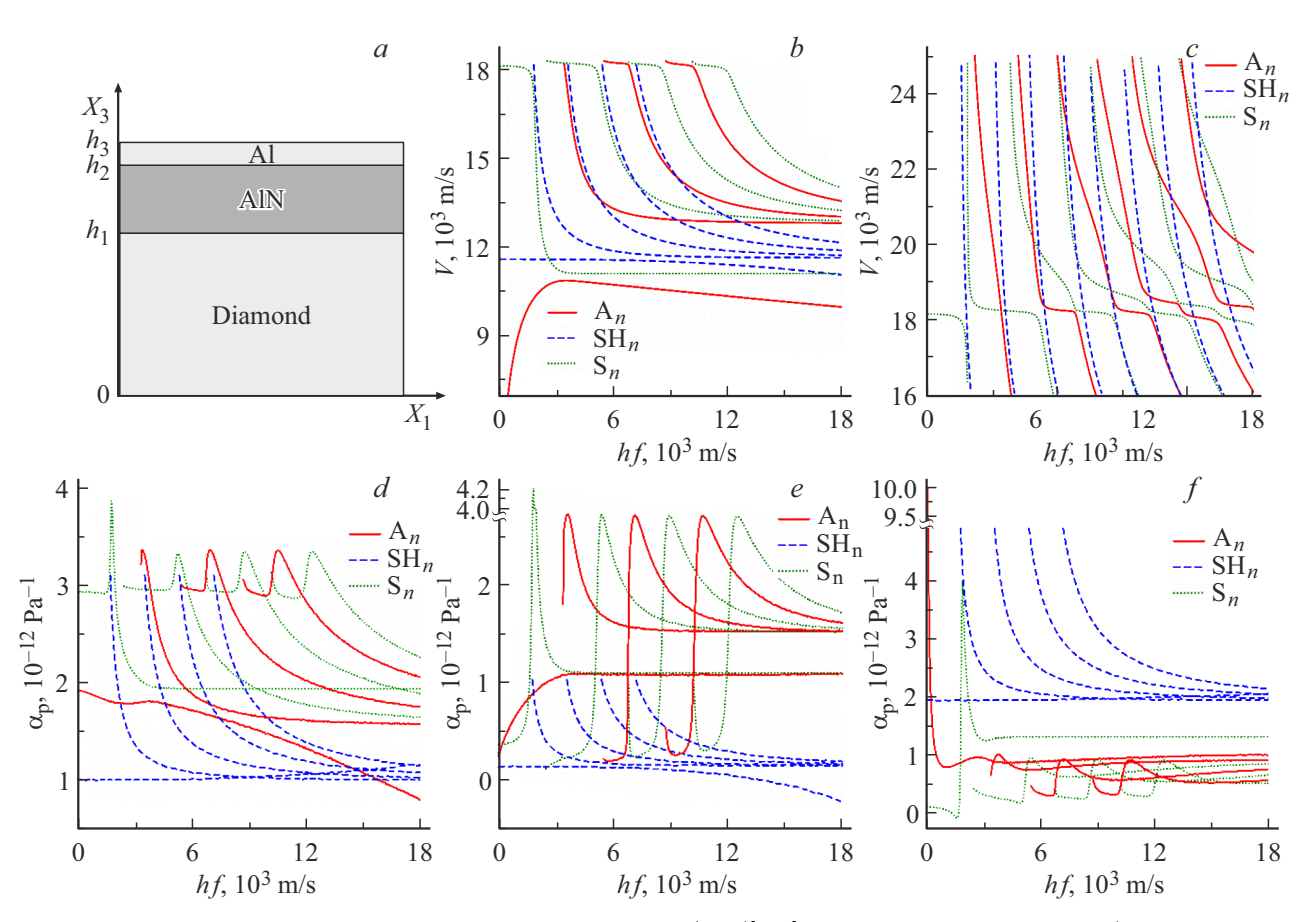


**Figure 1.** Dispersion dependences of elastic wave properties in the Al|AlN|[110]diamond multilayer structure. *a*) Arbitrary coordinate system; b, c) phase velocities; control coefficients (n = 1, 2, ...) for different pressure application cases: d)  $P \parallel X_1$ ; e)  $P \parallel X_2$ ; f)  $P \parallel X_3$ .

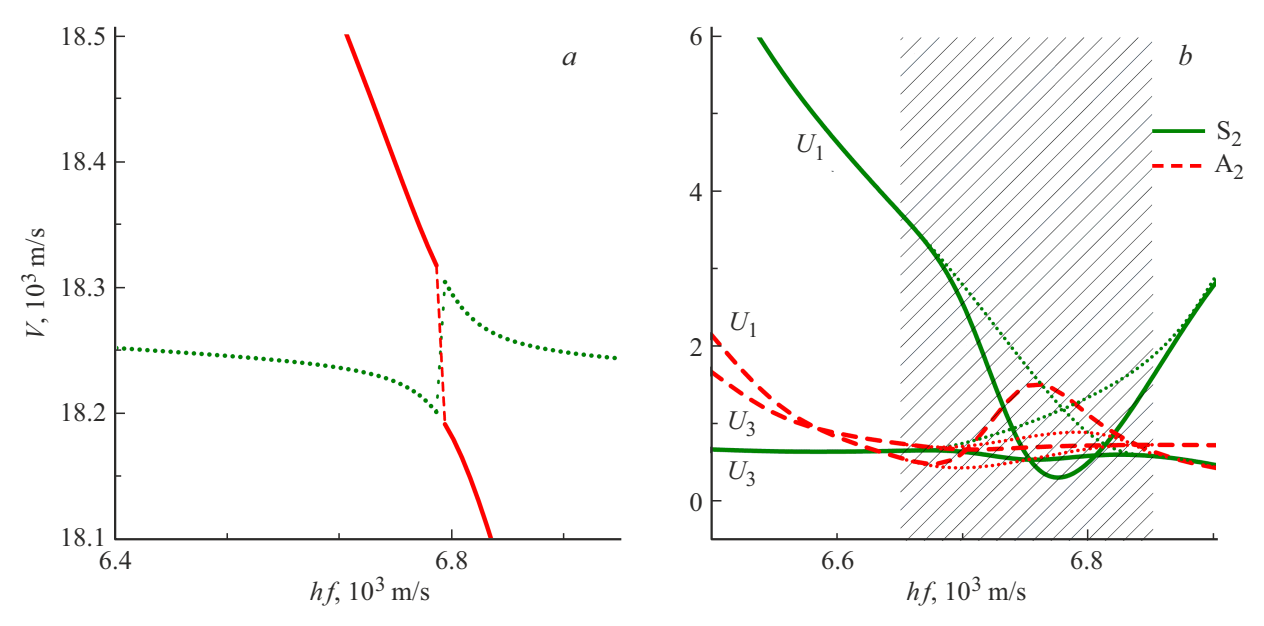
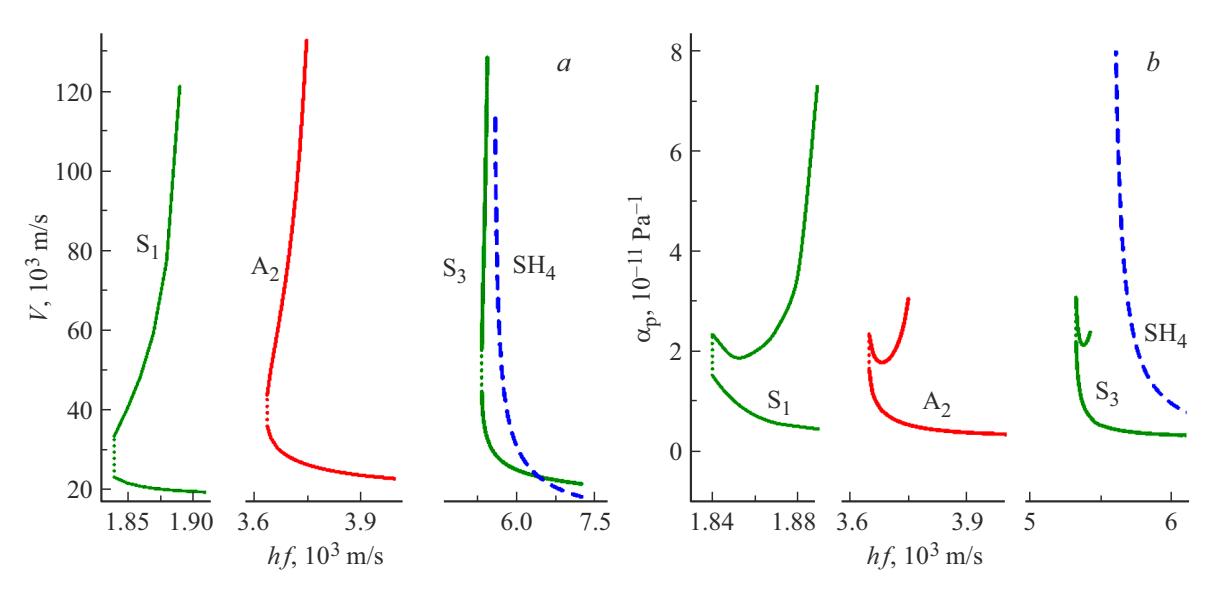


Figure 2. a) Phase velocities, b) components  $U_1$ ,  $U_3$  of the displacement vectors of the interacting Lamb wave modes  $A_2$  and  $S_2$ .

i.e. when PV is higher than the diamond's longitudinal BAW PV, hybridization occurs [31] between the Lamb wave modes  $A_1$  and  $S_1$ ,  $A_2$  and  $S_2$ ,  $A_3$  and  $S_3$ , etc. (Figure 1, c). In particular, hybridization between  $A_2$  and  $S_2$ 

occurs in the  $hf=6750\,\mathrm{m/s}$  region (Figure 2, a), where the type of interacting modes changes. The hybridization region is crosshatched in Figure 2, b. Note that, for the next interacting Lamb wave mode pairs, the degree of



**Figure 3.** Dispersion dependences of the Lamb wave back modes: a) phase velocities, b) control coefficients.

Maximum and minimum  $\alpha_p$  in the Al|AlN|[110]diamond structure exposed to the uniaxial mechanical pressure

Mode	Pressure direction	hf, m/s	$\alpha_{\rm p},10^{-12}{\rm Pa}^{-1}$
$S_0$		1850	3.88
$S_1$	$\mathbf{P} \parallel \mathbf{X}_1$	5400	3.30
$A_1$		3600	3.34
S <sub>0</sub>		1850	4.23
$A_1$	$\mathbf{P} \parallel \mathbf{X}_2$	3700	2.68
SH <sub>0</sub>		13 650	0
SH <sub>2</sub>		3200	5.25
S <sub>0</sub>	$\mathbf{P} \parallel \mathbf{X}_3$	1900	4
$\overline{S_2}$		3850	4.96

hybridization decreases as hf increases. Almost in any external uniaxial mechanical pressure application case, the degree of hybridization also decreases [32].

The given data may be used for choosing the best elastic wave propagation direction in the Al|AlN|[110]diamond structure exposed to the uniaxial mechanical pressure for creating controlled acoustoelectric devices. In particular, for  $A_1$ , where the wave PV  $\nu=17\,080.9\,\text{m/s}$  and signal delay in the 0.01 m line will be  $\Delta t=5.85\cdot 10^{-7}\,\text{s}$ , when  $P\parallel X_1$  is applied,  $\Delta t$  may vary within  $\pm 1.96\cdot 10^{-10}\,\text{s}$ , because  $\alpha_p=3.34\cdot 10^{-12}\,\text{Pa}^{-1}$ . The table provides some maximum and zero control coefficients in the Al|AlN|[110]diamond multilayer structure (Figure 1).

In the velocity region corresponding to membrane oscillations without energy transfer, the Al|AlN|[110]diamond structure has acoustic back waves [33] that, as mentioned

above, are characterized by negative energy transfer velocities in opposition to PV. Figure 3 shows the dispersion dependence of PV and  $\alpha_p$  of the acoustic back modes  $S_1$ ,  $A_2$ , and  $S_3$  of the Lamb wave. Frequency cutoff of the Lamb back waves for  $S_1$  takes place at  $hf=1840\,\mathrm{m/s}$ ,  $hf=3640\,\mathrm{m/s}$  is the  $A_2$  mode cutoff frequency and  $hf=5320\,\mathrm{m/s}$  is the  $S_3$  mode cutoff frequency.

Figure 3, b shows the dispersion dependences of  $\alpha_p$  of the Lamb back waves when the uniaxial mechanical pressure is applied along  $\mathbf{P} \parallel \mathbf{X}_1$ . In particular, in the ZGV region, the  $\alpha_p$  variation range is from  $1.53 \cdot 10^{-11}$  to  $2.35 \cdot 10^{-11}$  Pa<sup>-1</sup> for S<sub>1</sub>, but for S<sub>3</sub>, the  $\alpha_p$  variation range is from  $2.19 \cdot 10^{-11}$  to  $3.07 \cdot 10^{-11}$  Pa<sup>-1</sup>. However, for direct Lamb waves

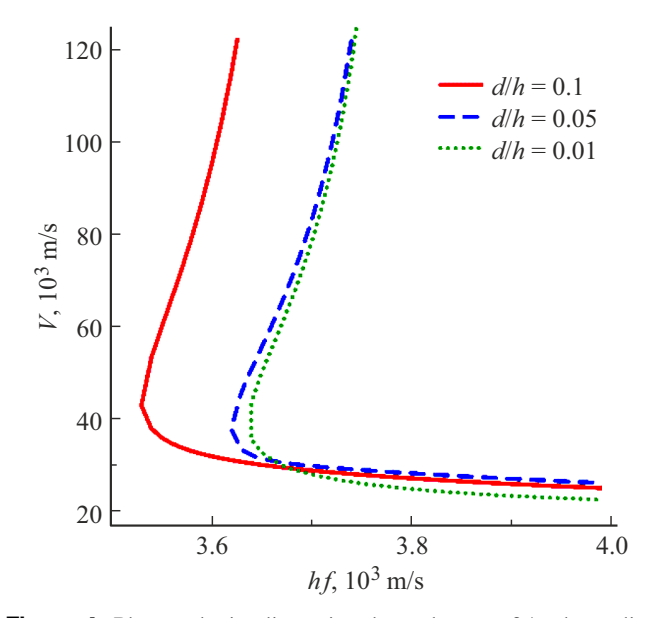


**Figure 4.** Phase velocity dispersion dependences of A<sub>2</sub> depending on the AlN|diamond thickness ratio.

in this PV range, values of  $\alpha_p$  have the same order, for example, SH<sub>4</sub> in Figure 3. Note that for other uniaxial mechanical pressure application cases, in particular, along the normal to the free surface  $\mathbf{P} \parallel \mathbf{X}_3$  or orthogonally to the sagittal plane of the surface  $\mathbf{P} \parallel \mathbf{X}_2$ , qualitative behavior of the dispersion curves of  $\alpha_p$  is the same (Figure 3, b); they differ only numerically. Note also a specific behavior of  $\alpha_p$  for back modes where  $\alpha_p$  first decreases in the ZGV point, but then starts growing as hf increases (Figure 3, b).

Application of the uniaxial mechanical pressure to the Al|AlN|[110]diamond structure has a little effect on the Lamb back wave cutoff frequency. The Lamb back wave cutoff frequency changes considerably when the layer thickness ration of the Al|AlN|[110]diamond structure changes. Figure 4 shows the PV dispersion dependences of  $A_2$  depending on the relation of the piezoelectric AlN thickness to the diamond thickness (d/h). Cutoff frequencies of  $A_2$  in this case hf are equal to 3540, 3630 and 3640 m/s for d/h 0.1, 0.05 and 0.01, respectively.

# 4. Conclusion

Application of the uniaxial mechanical pressure to Al|AlN|[110]diamond induces the modification of piezo-electric an dielectric constants of crystals leading to the modification of the elastic wave properties. The most considerable changes of the Lamb wave phase velocities are associated with mode interaction exhibited in the standing wave conditions. The influence of the uniaxial mechanical pressure on the Lamb back wave cutoff frequencies is very low in practice, but the relations of piezoelectric thickness to substrate thickness modify the cutoff frequencies considerably. Control coefficients for the standing wave modes (membrane oscillations) are also up to three orders of magnitude as high as those of the running Lamb waves.

Note that there are also values of hf where application of the uniaxial mechanical pressure to the Al|AlN|[110] diamond multilayer structure almost has no effect on the elastic wave mode PV variations, i.e. the control coefficients become equal to zero.

#### **Conflict of interest**

The authors declare that they have no conflict of interest.

### References

- [1] C.K. Kent, N. Ramakrishnan, H.P. Kesuma. IEEE Sensors J. **24**, *11*, 17337 (2024).
- [2] C.C.W. Ruppel. IEEE TUFFC 64, 9, 1390 (2017).
- [3] X. Li, W. Wang, S. Fan, Y. Yin, Y. Jia, Y. Liang, M. Liu. Sensors **20**, *9*, 2441 (2020).
- [4] Y. Zhang, Q. Tan, L. Zhang, W. Zhang, J. Xiong. J. Physics D: Appl. Phys. 53, 37, 375401 (2020).
- [5] D. Lu, Y. Zheng, A. Penirschke, R. Jakoby. IEEE Sensors J. 16, 1, 13 (2016).

- [6] D.S. Ballantine Jr, R.M. White, S.J. Martin, A.J. Ricco, G.C. Frye, E.T. Zellers, H. Wohltjen. Acoustic Wave Sensors: Theory, Design & Physico-Chemical Applications. Elsevier (1996). 437 p.
- [7] V.B. Raj, A.T. Nimal, Y. Parmar, M.U. Sharma, K. Sreenivas, V. Gupta. Sensors. Actuators B: Chem. 147, 2, 517 (2010).
- [8] S.T. Haider, M.A. Shah, D.G. Lee, S. Hur. IEEE Access 11, 58779 (2023).
- [9] J. Du, X. Jin, J. Wang. Acta Mechanica **192**, *1*, 169 (2007).
- [10] C. Othmani, H. Zhang. Compos. Struct. 240, 112085 (2020).
- [11] I.B. Salah, F. Takali, C. Othmani, A. Njeh. Int. J. Mech. Sci. 223, 107281 (2022).
- [12] S.K. Panja, S.C. Mandal. Waves. Random. Complex Media 32, 2, 1000 (2020).
- [13] N. Gandhi, J.E. Michaels, S.J. Lee. J. Acoust. Soc. Am. 132, 3,1284 (2012).
- [14] C. Othmani, H. Zhang, A.R. Kamali, C. Lü, F. Takali, B. Köhler. Arch. Appl. Mech. 92, 1, 21 (2022).
- [15] A.A. Maznev, A.G. Every. Appl. Phys. Lett. 95, 1, 011903 (2009).
- [16] I.E. Kuznetsova, V.G. Mozhaev, I.A. Nedospasov. J. Commun. Technol. Electron. 61, 11, 1305 (2016).
- [17] I.A. Viktorov. Rayleigh and Lamb Waves. Plenum Press, NY (1967). 154 p.
- [18] T. Liu, W. Karunasena, S. Kitipornchai, M. Veidt. J. Acoust. Soc. Am. 107, 1, 306 (2000).
- [19] M.H. Lu, C. Zhang, L. Feng, J. Zhao, Y.F. Chen, Y.W. Mao, J. Zi, Y.-Y. Zhu, S.-N. Zhu, N.B. Ming. Nature Mater. 6, 10, 744 (2007).
- [20] Q. Xie, S. Mezil, P.H. Otsuka, M. Tomoda, J. Laurent, O. Matsuda, O.B. Wright. Nature Commun. 10, 1, 2228 (2019).
- [21] C.M. Grünsteidl, I.A. Veres, T.W. Murray. J. Acoust. Soc. Am. 138, 1, 242 (2015).
- [22] D.A. Kiefer, B. Plestenjak, H. Gravenkamp, C. Prada. J. Acoust. Soc. Am. 153, 2, 1386 (2023).
- [23] V. Yantchev, L. Arapan, I. Katardjiev, V. Plessky. Appl. Phys. Lett. 99, 3, 033505 (2011).
- [24] B. Zaitsev, I. Kuznetsova, I. Nedospasov, A. Smirnov, A. Semyonov. J. Sound Vib. 442, 155 (2019).
- [25] K.S. Aleksandrov, Effectivnye piezoelektricheskie kristally dlya akustoelektriniki, piezoelektroniki i sensorov, t. 2. Sibirskoe otdelenie RAN, Novosibirsk (2008). 428 s. (in Russian).
- [26] S.I. Burkov, O.P. Zolotova, B.P. Sorokin, P.P. Turchin. Ultrasonics 55, 104 (2015).
- [27] S.I. Burkov, O.N. Pletnev, P.P. Turchin, O.P. Zolotova, B.P. Sorokin. J. Sib. Fed. Univ. Math. Phys. 14, 1, 105 (2021).
- [28] S.I. Burkov, O.N. Pletnev, P.P. Turchin, O.P. Zolotova, B.P. Sorokin. IEEE Trans. Ultrason. Ferroelectr. Freq. Control. 68, 10, 3234 (2021).
- [29] G.M. Kvashnin, B.P. Sorokin, S.I. Burkov. Acoust. Phys. 67, 1, 38 (2021).
- [30] B.P. Sorokin, D.V. Yashin, N.O. Asafiev, S.I. Burkov, M.S. Kuznetsov, N.V. Luparev, A.V. Golovanov. Ultrasonics 149, 107575 (2025).
- [31] I.E. Kuznetsova, B.D. Zaĭtsev, A.A. Teplykh, I.A. Borodina. Acoust. Phys. **53**, *1*, 64 (2007).
- [32] S.I. Burkov, O.P. Zolotova, B.P. Sorokin. IEEE Trans. UFFC 58, 1, 239 (2011).
- [33] B.D. Zaitsev, I.E. Kuznetsova, A.A. Teplykh, I.A. Borodina. IEEE Ultrason. Symp., 677 (2006). https://doi.org/10.1109/ULTSYM.2006.189

Translated by E.Ilinskaya